

A Unified Voxel Diffusion Module for Point Cloud 3D Object Detection

Qifeng Liu, Dawei Zhao, Yabo Dong, Linzhi Shang, Liang Xiao, Juan Wang, Kunlong Zhao, Dongming Lu, Qi Zhu

Abstract

Recent advances in point cloud object detection have increasingly adopted Transformer-based and State Space Models (SSMs), demonstrating strong performance. However, voxel-based representations in these models require strict consistency in input and output dimensions due to their serialized processing, which limits the spatial diffusion capability typically offered by convolutional operations. This limitation significantly affects detection accuracy. Inspired by CNN-based object detection architectures, we propose a novel Voxel Diffusion Module (VDM) to enhance voxel-level representation and diffusion in point cloud data. VDM is composed of sparse 3D convolutions, submanifold sparse convolutions, and residual connections. To ensure computational efficiency, the output feature maps are downsampled to one-fourth of the original input resolution. VDM serves two primary functions: (1) diffusing foreground voxel features through sparse 3D convolutions to enrich spatial context, and (2) aggregating fine-grained spatial information to strengthen voxel-wise feature representation. The enhanced voxel features produced by VDM can be seamlessly integrated into mainstream Transformer- or SSM-based detection models for accurate object classification and localization, highlighting the generalizability of our method. We evaluate VDM on several benchmark datasets by embedding it into both Transformer-based and SSM-based models. Experimental results show that our approach consistently improves detection accuracy over baseline models. Specifically, VDM-SSMs achieve 74.7 mAPH (L2) on Waymo, 72.9 NDS on nuScenes, 42.3 mAP on Argoverse 2, and 67.6 mAP on ONCE, setting new state-of-the-art performance across all datasets. Our code will be made publicly available.

Introduction

3D object detection based on point clouds plays a crucial role in applications such as autonomous driving (Bansal, Krizhevsky, and Ogale 2018) and robotic navigation (Zhu et al. 2017). Inspired by the remarkable success of Transformers (Vaswani et al. 2017) and State Space Models (SSMs) (Gu and Dao 2023) in natural language processing, researchers have recently explored adapting these architectures to computer vision tasks, achieving strong performance. For example, in the domain of point cloud 3D object detection, DVST (Wang et al. 2023) introduces a dynamic sparse window attention mechanism that adaptively partitions each window into local sub-regions based

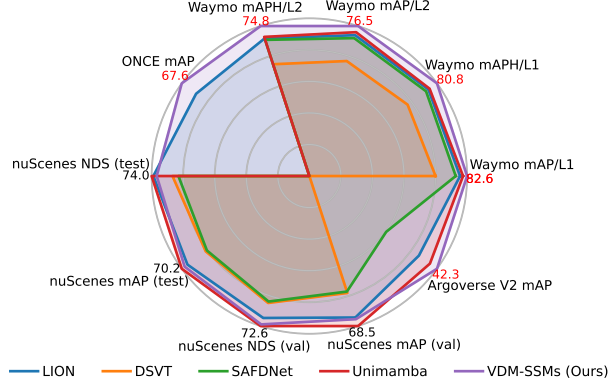


Figure 1: Performance comparison of different models on various datasets. Numbers highlighted in red indicate that our model achieves state-of-the-art results.

on voxel sparsity, enabling fully parallel attention computations. LION (Liu et al. 2024) further extends this direction by employing large grouping windows and leveraging SSMs' ability to capture long-range voxel dependencies, setting new state-of-the-art (SOTA) performance on several public datasets. Despite these advancements, both Transformer-based and SSM-based models for point cloud voxel sequence processing require consistency in input and output sequence dimensions, which fundamentally limits their ability to perform convolution-like spatial diffusion. However, prior work (Zhang et al. 2024a; Liu et al. 2024) has demonstrated that voxel diffusion, particularly for foreground voxels, is critical for enhancing detection accuracy. For instance, LION selects top- k voxels via feature summation and applies directional diffusion during intermediate processing. In contrast, our method proposes to conduct voxel diffusion *before* serialization, using convolutional operations to enrich the original voxel space with contextually relevant features.

Motivated by CNN-based object detection architectures, we propose a novel **Voxel Diffusion Module (VDM)** tailored for both Mamba-based and Transformer-based 3D detection models. Positioned before voxel sequence serialization, VDM leverages 3D convolutional operations to diffuse foreground voxel features and increase their spatial density.

Simultaneously, sparse convolutions are employed to aggregate fine-grained spatial features within each voxel’s local 3D neighborhood, supplying the downstream sequence model with richer spatial context. Structurally, VDM consists of stacked sparse 3D convolutions and residual blocks, effectively supporting both diffusion and aggregation. The output feature map is downsampled to one-fourth of the input resolution (in height and width), helping reduce the computational load for subsequent models.

VDM is designed to be modular and general, allowing seamless integration with both Transformer-based and SSM-based detectors. To evaluate its effectiveness, we perform extensive experiments on four large-scale datasets. As shown in Figure 1, our VDM-enhanced SSM-based model (VDM-Mamba) achieves **74.7 mAPH (L2)** on Waymo, **68.1 mAP** on nuScenes, **42.3 mAP** on Argoverse 2, and **67.6 mAP** on ONCE, setting a new state-of-the-art (SOTA) performance. Additionally, the Transformer-based variant (VDM-DSVT) improves performance by **+2.2 mAPH (L2)** over the DSVT baseline on the Waymo dataset, confirming the general effectiveness of our approach.

Our contributions can be summarized as follows:

- We propose **VDM**, a voxel diffusion module that enhances the representation of raw voxel inputs through 3D convolution, significantly enriching foreground voxel features and improving detection accuracy.
- VDM utilizes sparse 3D convolutions and residual networks to aggregate spatial features from the voxel neighborhood, providing richer positional cues for downstream sequence modeling.
- VDM is a general-purpose module that integrates well with both Transformer-based and SSM-based 3D detectors, consistently boosting model performance.
- We validate the effectiveness of VDM through experiments on multiple public datasets, where VDM-SSMs achieve SOTA results, and VDM also improves Transformer-based models.

Related Work

3D object detection based on point clouds has seen significant progress in recent years. According to model architecture, existing approaches can be broadly categorized into three types: CNN-based, Transformer-based, and SSM-based methods. CNN-based models emerged earlier and have been thoroughly studied, achieving solid performance. In contrast, Transformer and Mamba-based models are relatively recent, and while less explored for 3D object detection, they have already shown promising results—often surpassing CNN-based methods in detection accuracy.

CNN-Based 3D Object Detection. CNN-based 3D detectors are typically categorized into voxel-based and point-based approaches. VoxelNet (Zhou and Tuzel 2018) introduces a Voxel Feature Encoding (VFE) layer to convert point clusters within voxels into unified feature representations. HEDNet uses an encoder-decoder design to capture long-range spatial dependencies, particularly useful for detecting large or distant objects. SAFDNet proposes an

adaptive feature diffusion strategy to address missing center features in sparse detectors. PointPillars (Lang et al. 2019) leverages PointNet to learn features from vertical columns of point clouds, offering notable inference speed advantages. CenterPoint (Yin, Zhou, and Krahenbuhl 2021) detects object centers using a keypoint detector and regresses attributes such as 3D size, orientation, and velocity. 3DSSD (Yang et al. 2020) introduces a fused sampling strategy in the downsampling process to retain informative representative points. IASSD (Zhang et al. 2022) proposes two task-aware, instance-sensitive sampling strategies for hierarchically selecting foreground points of interest. Among these approaches, voxel-based detectors generally achieve higher accuracy and have become the dominant choice for outdoor 3D detection tasks.

Transformer-Based 3D Object Detection. Transformers have achieved state-of-the-art performance in both NLP and computer vision tasks. PVT-SSD (Yang et al. 2023) introduces a Point-Voxel Transformer that captures long-range dependencies via voxel tokens while preserving fine spatial detail through point-level features. FlatFormer (Liu et al. 2023) flattens point clouds using window-based sorting and partitions them into equal-sized groups, improving detection efficiency. DSVT (Wang et al. 2023) proposes a Dynamic Sparse Window Attention mechanism that adaptively splits each window based on voxel sparsity, enabling fully parallel feature computation. However, the serialization of voxel features in Transformer-based methods can lead to the loss of fine-grained spatial cues, limiting performance in complex 3D scenes.

SSM-Based 3D Object Detection. SSM-based detectors represent a new and emerging line of work. LION (Liu et al. 2024) applies a large-group strategy during voxel serialization for more effective spatial context modeling. Voxel Mamba (Zhang et al. 2024b) eliminates the grouping step and serializes the entire voxel space as a single sequence, introducing a Dual-Scale SSM Block to capture hierarchical spatial dependencies. UniMamba combines 3D convolution with SSMs in a compact multi-head architecture that efficiently captures both local and global spatial context.

Although still in their early stages, SSM-based models already outperform traditional CNN-based frameworks on several benchmarks due to their strong modeling capabilities. Our proposed Voxel Diffusion Module (VDM) further enhances these serialized architectures by introducing voxel diffusion and fine-grained spatial feature aggregation prior to serialization. This design supplies Transformer- and SSM-based models with richer input representations, leading to significant performance gains in 3D object detection.

Method

In this section, we introduce the proposed Voxel Diffusion Module (VDM), designed to enhance the representation of voxelized point cloud features. VDM leverages convolutional operations to perform early-stage voxel diffusion, increasing the density of meaningful voxel information. This provides richer input for downstream serialized models such as Transformers or Mamba. Furthermore, VDM aggregates

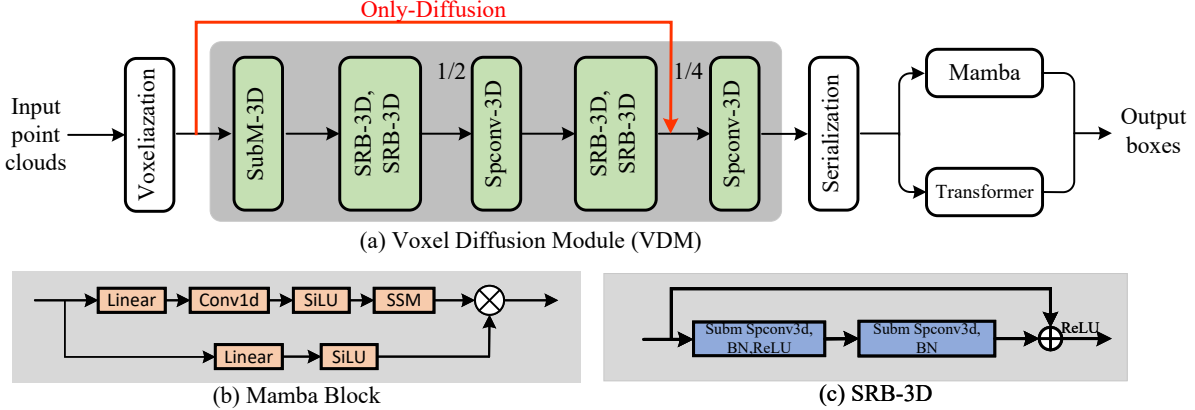


Figure 2: Overall architecture of our proposed method. (a) The Voxel Diffusion Module (VDM) is placed before the sequential detection model, enabling diffusion of raw voxelized point clouds and aggregation of spatial voxel features. Internally, it consists of Submanifold 3D Convolution (SubM3D), Sparse Residual Block (SRB-3D), and Sparse 3D Convolution (SPConv-3D), where SPConv-3D plays a key role in voxel diffusion. (b) Mamba Block. (c) Sparse Residual Block (SRB-3D). The red connection line "Only-Diffusion" in the figure indicates the model architecture when only the voxel diffusion strategy is applied in the VDM, aiming to highlight the critical impact of voxel diffusion on detection performance.

local spatial features within each voxel’s 3D neighborhood, enabling the sequence models to more effectively utilize spatial positional cues during processing.

Preliminaries

Transformer. Transformers, based on self-attention mechanisms, have been widely adopted in both natural language processing and computer vision. The standard attention mechanism is defined as:

$$\text{Attention}(Q, K, V) = \text{softmax} \left(\frac{QK^\top}{\sqrt{d_k}} \right) V \quad (1)$$

Here, Q (Query), K (Key), and V (Value) represent the input projection vectors. Q interacts with K^\top to compute similarity scores, which are then used to weight the values in V . The term d_k denotes the dimensionality of the key vectors, and the scaling factor $\sqrt{d_k}$ is introduced to stabilize the gradients during training. While Transformers are powerful in capturing global dependencies, their quadratic time complexity poses a challenge when handling long sequences, such as in voxelized point clouds.

State Space Models (SSMs). SSMs model sequential data through continuous-time state equations:

$$h'(t) = Ah(t) + Bx(t) \quad (2)$$

$$y(t) = Ch(t) \quad (3)$$

where $x(t) \in \mathbb{R}^L$ is the continuous input signal, $y(t) \in \mathbb{R}^L$ is the output, and $A \in \mathbb{R}^{N \times N}$, $B \in \mathbb{R}^{N \times 1}$, and $C \in \mathbb{R}^{1 \times N}$ are learnable parameters. The discrete form is expressed as:

$$h_t = A'h_{t-1} + B'x_t \quad (4)$$

$$y_t = Ch_t \quad (5)$$

where A' and B' are obtained from continuous A and B via a discretization rule: $A' = f_A(\Delta, A)$ and $B' = f_B(\Delta, A, B)$. Mamba-based SSM models (Gu and Dao 2023) have demonstrated significant advantages over Transformers in terms of modeling long-range dependencies and computational efficiency. In the context of 3D point cloud detection, such models (Jin et al. 2025; Liu et al. 2024) have shown promising results and even outperformed many Transformer-based architectures.

Sparse Residual Block (SRB). In CNN-based 3D detectors such as SAFDNet (Zhang et al. 2024a), the Sparse Residual Block (SRB) is commonly used for efficient feature extraction. An SRB consists of two 3D submanifold sparse convolution layers and a residual skip connection linking the input to the output. In our design, VDM is composed of stacked SRB modules and additional SubM3D layers to enable both voxel diffusion and spatial feature aggregation. This structure facilitates the enrichment of voxel-level spatial representations before they are passed into the serialized backbone (Transformer or SSM), thereby improving detection accuracy.

Overall Architecture

As illustrated in Figure 2, the Voxel Diffusion Module (VDM) is designed to perform voxel-level diffusion of point clouds and aggregate fine-grained voxel features. This facilitates the generation of rich foreground voxel representations and fine-grained spatial features, serving as a beneficial foundation for subsequent transformer-based and state-space model (SSM)-based detectors. Convolutional neural network (CNN)-based models (Zhang et al. 2024a) have

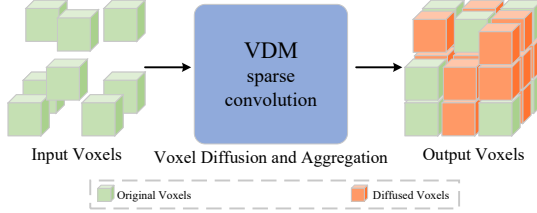


Figure 3: Visualization of the Voxel Diffusion Module (VDM) applied to the original point clouds, demonstrating its effect in voxel-level diffusion and feature aggregation.

been extensively studied in 3D object detection. These models typically begin by applying feature extraction networks to voxelized point clouds, followed by a backbone and a detection head for final predictions. Inspired by this paradigm, the proposed VDM is composed of alternating Submanifold 3D Convolution (SubM3D) layers and Sparse Residual Blocks (SRB). Additionally, two Sparse 3D Convolution (SPConv3D) layers are inserted to downsample and upsample the voxel feature maps, enabling hierarchical feature learning and effective diffusion.

Voxel Diffusion in VDM. Voxel diffusion plays a significant role in enhancing model detection performance, as demonstrated in previous studies (Liu et al. 2024; Zhang et al. 2024a). Inspired by the property of convolution operations to increase the number of sparse features, we introduce a sparse 3D convolution with a kernel size of 3 within our proposed Voxel Diffusion Module (VDM). This module enables diffusion over the input voxel grid, thus expanding the spatial distribution of informative voxels. Figure 3 illustrates how VDM diffuses the original point cloud into a denser voxel representation, providing a richer feature basis for subsequent serial detection networks. To quantitatively evaluate this effect, we perform a statistical analysis on the voxel count post-VDM processing, as shown in Table 1. As observed, the number of total and foreground voxels significantly increases after applying VDM. This expansion ensures that subsequent modules—particularly those based on transformers or State Space Models (SSMs)—can access more comprehensive foreground point features, thereby improving object detection accuracy. It is worth noting that voxel diffusion serves as a crucial component of the VDM. Our later experiments will further highlight its contribution to performance gains, underlining its importance in boosting the effectiveness of serialization-based architectures such as transformers and Mamba variants.

Fine-Grained Feature Aggregation. To capture more detailed spatial information, we further divide the voxel grid into finer partitions, as illustrated in Figure 4. Leveraging the strong spatial perception capabilities of the Submanifold 3D Convolution (SubM3D) and the Sparse Residual Block (SRB) within the VDM, we extract fine-grained voxel features from these subdivided regions. In addition, we adopt a sparse convolution with a stride of 2 to serve dual pur-

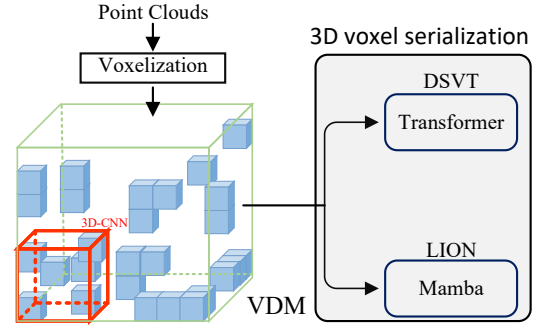


Figure 4: Fine-grained feature aggregation within the VDM, utilizing convolutional operations to aggregate relative spatial information across voxels.

Method	Overall Voxel Count	Foreground Voxel Count	mAPH L2
Non(LION)	36340	2616	74.0
VDM	188562	9146	74.8
VDM(OD)	216601	10705	74.8

Table 1: Effect of VDM on voxel counts in input point clouds on the Waymo validation dataset. The overall and foreground voxel counts are computed as the total number of corresponding voxels across all frames divided by the total number of frames.

poses: first, it reduces the resolution of the feature map to half, which effectively controls computational cost by mitigating the overhead introduced by voxel diffusion; second, it aggregates local fine-grained features, thereby enriching the spatial context available for downstream modules. This design ensures that the model benefits from both detailed spatial representations and efficient computation during object detection.

The function of VDM is to diffuse the number of sparse voxels and to aggregate fine-grained features. It can be summarized by the following formulas:

$$FG' = \text{Voxel_Diffusion}(FG, spconv) \quad (6)$$

$$F' = \text{Aggregation}(F, subm, spconv) \quad (7)$$

where F denotes the initial voxel feature map; F' represents the feature map after local voxel aggregation, with width and height reduced to one-fourth of the original size; $subm$ denotes submanifold sparse convolution, and $spconv$ denotes sparse convolution. FG' indicates the number of foreground voxels after VDM processing, and FG is the number of foreground voxels in the initial feature map.

Integration with SSMs and Transformer Modules. The proposed VDM module can be integrated with both Mamba-based and Transformer-based models. By effectively diffusing sparse voxels and aggregating fine-grained point cloud voxel features, VDM further enhances the detection accuracy of the overall model. For the 3D feature maps processed by VDM, we first serialize them into one-dimensional sequences along the x and y directions. As the sequence

Methods	Operator	Vehicle 3D AP/APH		Pedestrian 3D AP/APH		Cyclist 3D AP/APH		mAP/mAPH (L2)
		L1	L2	L1	L2	L1	L2	
SECOND	CNN	72.3/71.7	63.9/63.3	68.7/58.2	60.7/51.3	60.6/59.3	58.3/57.0	61.0/57.2
PointPillars		72.1/71.5	63.6/63.1	70.6/56.7	62.8/50.3	64.4/62.3	61.9/59.9	62.8/57.8
CenterPoint		74.2/73.6	66.2/65.7	76.6/70.5	68.8/63.2	72.3/71.1	69.7/68.5	68.2/65.8
PV-RCNN		78.0/77.5	69.4/69.0	79.2/73.0	70.4/64.7	71.5/70.3	69.0/67.8	69.6/67.2
PillarNet-18		78.2/77.7	70.4/69.9	79.8/72.6	71.6/64.9	70.4/69.3	67.8/66.7	69.9/67.2
FSD		79.2/78.8	70.5/70.1	82.6/77.3	73.9/69.1	77.1/76.0	74.4/73.3	72.9/70.8
AFDetV2		77.6/77.1	69.7/69.2	80.2/74.6	72.2/67.0	73.7/72.7	71.0/70.1	71.0/68.8
PillarNeXt		78.4/77.9	70.3/69.8	82.5/77.1	74.9/69.8	73.2/72.2	70.6/69.6	71.9/69.7
VoxelNext		78.2/77.7	69.9/69.4	81.5/76.3	73.5/68.6	76.1/74.9	73.3/72.2	72.2/70.1
CenterFormer		75.0/74.4	69.9/69.4	78.6/73.0	73.6/68.3	72.3/71.3	69.8/68.8	71.1/68.9
PV-RCNN++		79.3/78.8	70.6/70.2	81.3/76.3	73.2/68.0	73.7/72.7	71.2/70.2	71.7/69.5
ConQueR		76.1/75.6	68.7/68.2	79.0/72.3	70.9/64.7	73.9/72.5	71.4/70.1	70.3/67.7
FocalFormer3D		—/—	68.1/67.6	—/—	72.7/66.8	—/—	73.7/72.6	71.5/69.0
HEDNet		81.1/80.6	73.2/72.7	84.4/80.0	76.8/72.6	78.7/77.7	75.8/74.9	75.3/73.4
VPF		80.2/79.7	71.9/71.5	82.5/76.9	74.8/69.4	77.1/76.0	74.2/73.2	73.6/71.4
TransFusion	Transformer	—/—	—/65.1	—/—	—/63.7	—/—	—/65.9	—/64.9
SST-TS		76.2/75.8	68.0/67.6	81.4/74.0	72.8/65.9	—/—	—/—	—/—
SWFormer		77.8/77.3	69.2/68.8	80.9/72.7	72.5/64.9	—/—	—/—	—/—
FlatFormer		—	69.0/68.6	—	71.5/65.3	—/—	68.6/67.5	69.7/67.2
OcTr		78.1/77.6	69.8/69.3	80.8/74.4	72.5/66.5	72.6/71.5	69.9/68.9	70.7/68.2
DSVT-Pillar		79.3/78.8	70.9/70.5	82.8/77.0	75.2/69.8	76.4/75.4	73.6/72.7	73.2/71.0
DSVT-Voxel		79.2/78.8	70.9/70.5	82.9/77.7	75.2/70.3	77.2/76.2	74.3/73.4	73.5/71.4
VDM-DSVT(Ours)		79.7/79.3	71.4/71.0	84.3/79.7	76.7/72.3	78.4/77.4	75.6/74.6	74.6/72.6
Voxel Mamba	SSMs	80.8/80.3	72.6/72.2	85.0/80.8	77.7/73.6	78.6/77.6	75.7/74.8	75.3/73.6
LION		80.3/79.9	72.0/71.6	85.8/81.4	78.5/74.3	80.1/79.0	77.2/76.2	75.9/74.0
UniMamba		80.6/80.1	72.3/71.8	86.0/81.3	78.7/74.1	80.3/79.3	77.5/76.5	76.1/74.1
VDM-Mamba (Ours)		81.0/80.5	72.6/72.2	86.4/82.5	79.3/75.5	80.4/79.4	77.5/76.5	76.5/74.8
VDM-OD-Mamba (Ours)		81.3/80.9	73.0/72.6	86.1/82.1	78.9/75.0	80.7/79.7	77.8/76.9	76.6/74.8

Table 2: Comparison with prior methods (CNNs, Transformers, and SSMs) on the Waymo Open Dataset using 100% training data. Metrics are reported as mAP/mAPH (%) ↑ for overall results and AP/APH (%) ↑ per category. All models are trained under the single-frame setting. “—” indicates unavailable results. VDM-OD-Mamba denotes a variant where the Only-Diffusion structure is used within the VDM framework. The best-performing results are highlighted in bold.

length increases, Mamba-based networks are able to adopt larger grouping sizes due to their lower computational complexity compared to Transformer-based counterparts. Given the strong performance of LION (Liu et al. 2024) and DSVT (Wang et al. 2023) in the field of 3D object detection, we integrate the VDM module into both networks and conduct experiments to validate its effectiveness.

Experiments

Datasets and Evaluation Metrics

Waymo Open Dataset. The Waymo Open Dataset (WOD) (Sun et al. 2020) includes 1,150 scenes, divided into 798 for training, 202 for validation, and 150 for testing. Each scene covers a perception range of 150 m × 150 m. For evaluation, WOD adopts 3D mean Average Precision (mAP) and mAP weighted by heading accuracy (mAPH). Each metric includes two difficulty levels: L1 for objects with more than five points, and L2 for bounding boxes containing one to five points.

nuScenes Dataset. The nuScenes dataset (Caesar et al. 2020) contains 1,000 scenes, with 750 for training, 150 for

validation, and 150 for testing. It uses mean Average Precision (mAP) and nuScenes Detection Score (NDS) as evaluation metrics. The dataset covers 10 annotated object classes, representing most common categories in traffic scenarios.

Argoverse 2 Dataset. The Argoverse 2 dataset (Chang et al. 2019) comprises 1,000 sequences, with 700 for training, 150 for validation, and 150 for testing. The perception range extends up to 200 meters. It uses mean Average Precision (mAP) as the evaluation metric.

ONCE Dataset. The ONCE dataset (Mao et al. 2021) consists of 5,000, 3,000, and 8,000 frames for training, validation, and testing respectively. It defines three detection classes: Vehicle, Pedestrian, and Cyclist. The final performance is evaluated using mean Average Precision (mAP) across all three classes.

Implementation Details

Network Architecture. We evaluate the proposed VDM module by integrating it with both the SSMs-based LION (Liu et al. 2024) and the Transformer-based DSVT (Wang et al. 2023) models. We use voxel sizes of (0.075 m, 0.075 m, 0.25 m), (0.08 m, 0.08 m, 0.1875 m),

Performances on the validation set												
Method	NDS	mAP	Car	Truck	Bus	T.L.	C.V.	Ped.	M.T.	Bike	T.C.	B.R.
CenterPoint	66.5	59.2	84.9	57.4	70.7	38.1	16.9	85.1	59.0	42.0	69.8	68.3
VoxelNeXt	66.7	60.5	83.9	55.5	70.5	38.1	21.1	84.6	62.8	50.0	69.4	69.4
Uni3DETR	68.5	61.7	—	—	—	—	—	—	—	—	—	—
Transfusion-LiDAR	70.1	65.5	86.9	60.8	73.1	43.4	25.2	87.5	72.9	57.3	77.2	70.3
DSVT	71.1	66.4	87.4	62.6	75.9	42.1	25.3	88.2	74.8	58.7	77.9	71.0
HEDNet	71.4	66.7	87.7	60.6	77.8	50.7	28.9	87.1	74.3	56.8	76.3	66.9
SAFDNet	71.0	66.3	87.6	60.8	78.0	43.5	26.6	87.8	75.5	58.0	75.0	69.7
LION	72.1	68.0	87.9	64.9	77.6	44.4	28.5	89.6	75.6	59.4	80.8	71.6
UniMamba	72.6	68.5	88.7	64.7	79.7	47.9	28.7	89.7	74.6	59.1	79.5	72.3
VDM-mamba(Ours)	72.5	68.1	88.5	59.5	78.8	43.2	30.6	90.2	75.2	61.1	81.4	72.5
VDM-OD-mamba(Ours)	72.9	68.5	88.7	65.7	78.9	43.8	29.7	90.2	75.7	60.9	81.1	70.3
Performances on the test set												
TransFusion-LiDAR	70.2	65.5	86.2	56.7	66.3	58.8	28.2	86.1	68.3	44.2	82.0	78.2
DSVT	72.7	68.4	86.8	58.4	67.3	63.1	37.1	88.0	73.0	47.2	84.9	78.4
HEDNet	72.0	67.7	87.1	56.5	70.4	63.5	33.6	87.9	70.4	44.8	85.1	78.1
VPF	72.7	67.0	85.8	55.1	63.5	62.1	33.3	87.6	72.5	48.6	82.9	78.2
SAFDNet	72.3	68.3	87.3	57.3	68.0	63.7	37.3	89.0	71.1	44.8	84.9	79.5
LION	73.9	69.8	87.2	61.1	68.9	65.0	36.3	90.0	74.0	49.2	87.3	79.5
VDM-mamba(Ours)	73.7	70.0	88.0	60.1	67.6	66.0	35.1	90.9	72.2	50.9	89.2	80.0

Table 3: Performances on the nuScenes validation and test set. ‘T.L.’, ‘C.V.’, ‘Ped.’, ‘M.T.’, ‘T.C.’, and ‘B.R.’ are short for trailer, construction vehicle, pedestrian, motor, traffic cone, and barrier, respectively. VDM-OD-Mamba denotes a variant where the Only-Diffusion structure is used within the VDM framework.

(0.1 m, 0.1 m, 0.25 m), and (0.1 m, 0.1 m, 0.25 m) for the nuScenes, Waymo, Argoverse 2, and ONCE datasets respectively. The number of voxel feature channels is set to 64.

In the VDM module, the SubM3D (including SRB) layers use a kernel size of 3. All SparseConv3D layers adopt a kernel size of 3, stride of 2, and padding of 1 to downsample the feature map resolution. The channel configurations within VDM are set as (64, 32), (32, 64), and (64, 128).

For LION and DSVT, we follow the default parameter settings from their original papers without modification. Additionally, we conduct an *only-diffusion* experiment, in which the voxel size along the *x* and *y* axes is scaled by a factor of 4, while the *z* axis remains unchanged.

Training Process. We train all models using 8 NVIDIA A40 GPUs. On the Waymo Open Dataset, the VDM-SSMs configuration is trained for 24 epochs with a batch size of 16, while the VDM-DSVT configuration uses 24 epochs with a batch size of 8. For the remaining three datasets, we adopt the same training strategy as that used in the LION (Liu et al. 2024) baseline.

Main Results

To verify the effectiveness of the proposed module, we design two models: VDM-SSMs based on LION and VDM-Transformer based on DSVT. We evaluate their performance on four benchmark datasets: Waymo, nuScenes, Argoverse V2, and ONCE.

Results on WOD. As shown in Table 2, we incorporate the VDM module into both Mamba-based and Transformer-based models. Among them, VDM-Mamba achieves a state-of-the-art (SOTA) result of 74.8 mAPH (L2), outperforming

the corresponding baseline LION model (without VDM) by +0.7 mAPH, and also surpassing the recent UniMamba (Jin et al. 2025).

In addition, VDM-DSVT also demonstrates performance gains, achieving a +1.2 mAPH (L2) improvement over the original DSVT, which validates the general applicability of the VDM module to both SSM-based and Transformer-based detectors.

When only the diffusion mechanism is retained in VDM (i.e., VDM-OD-Mamba), the model still achieves the best results on the Vehicle and Cyclist categories, highlighting the importance of the diffusion component in the overall design. Moreover, VDM-Mamba achieves the best performance in the Pedestrian category, suggesting that the fine-grained aggregation ability introduced by VDM is particularly beneficial for small object detection.

Results on nuScenes. To further verify the effectiveness of the proposed VDM module, we conduct experiments on both the nuScenes validation and test sets. As shown in Table 3, VDM-mamba achieves 68.1 mAP and 72.5 NDS on the validation set, and 70.0 mAP and 73.7 NDS on the test set.

Although VDM-mamba slightly underperforms UniMamba in terms of overall detection accuracy, it achieves the best results in the pedestrian and bicycle categories on the nuScenes validation set. These categories are particularly important for autonomous driving applications, demonstrating that our proposed method offers clear advantages in detecting small and vulnerable objects. Furthermore, VDM-OD-Mamba achieves a state-of-the-art 72.9 NDS, suggesting that the diffusion-only structure plays a critical role in

Method	mAP	Vehicle	Bus	Pedestrian	Stop Sign	Box Truck	Bollard	C-Barrel	Motorcyclist	MPC-Sign	Motorcycle	Bicycle	A-Bus	Shool Bus	Truck Cab	C-Cone	V-Trailer	Sign	Large Vehicle	Stroller	Bicyclist	Truck	MBT	Dog	Wheelchair	W-Device	W-Rider
CenterPoint	22.0	67.6	38.9	46.5	16.9	37.4	40.1	32.2	28.6	27.4	33.4	24.5	8.7	25.8	22.6	29.5	22.4	6.3	3.9	0.5	20.1	22.1	0.0	3.9	0.5	10.9	4.2
HEDNet	37.1	78.2	47.7	67.6	46.4	45.9	56.9	67.0	48.7	46.5	58.2	47.5	23.3	40.9	27.5	46.8	27.9	20.6	6.9	27.2	38.7	21.6	0.0	30.7	9.5	28.5	8.7
VoxelNeXt	30.7	72.7	38.8	63.2	40.2	40.1	53.9	64.9	44.7	39.4	42.4	40.6	20.1	25.2	19.9	44.9	20.9	14.9	6.8	15.7	32.4	16.9	0.0	14.4	0.1	17.4	6.6
FSDV2	37.6	77.0	47.6	70.5	43.6	41.5	53.9	58.5	56.8	39.0	60.7	49.4	28.4	41.9	30.2	44.9	33.4	16.6	7.3	32.5	45.9	24.0	1.0	12.6	17.1	26.3	17.2
SAFDNNet	39.7	78.5	49.4	70.7	51.5	44.7	65.7	72.3	54.3	49.7	60.8	50.0	31.3	44.9	24.7	55.4	31.4	22.1	7.1	31.1	42.7	23.6	0.0	26.1	1.4	30.2	11.5
LION	41.5	75.1	43.6	73.9	53.9	45.1	66.4	74.7	61.3	48.7	65.1	56.2	21.7	42.7	25.3	58.4	28.9	23.6	8.3	49.5	47.3	19.0	0.0	31.4	8.7	37.6	11.8
UniMamba	42.0	78.9	47.9	74.3	51.8	46.8	67.8	76.9	55.8	51.7	62.8	52.2	30.2	44.6	24.6	28.1	59.4	32.2	23.2	6.7	41.5	48.5	0.0	26.4	8.1	36.4	13.7
VDM (Ours)	42.3	78.2	48.2	75.2	53.2	45.7	68.2	77.4	60.3	47.2	67.0	58.0	24.9	43.0	24.9	60.1	31.4	25.1	7.8	42.5	46.3	20.9	0.0	29.7	10.3	39.8	13.6
VDM-OD(Ours)	42.6	79.0	49.5	75.9	54.5	45.5	69.9	77.9	56.9	47.6	66.6	59.2	24.0	44.2	24.7	60.9	33.2	24.9	7.5	39.5	51.3	20.1	0.0	33.7	7.8	40.1	12.5

Table 4: Comparison with prior methods on the Argoverse2 validation set. ‘Vehicle’, ‘C-Barrel’, ‘MPC-Sign’, ‘A-Bus’, ‘C-Cone’, ‘V-Trailer’, ‘MBT’, ‘W-Device’, and ‘W-Rider’ are abbreviations for regular vehicle, construction barrel, mobile pedestrian crossing sign, articulated bus, construction cone, vehicular trailer, message board trailer, wheeled device, and wheeled rider, respectively. **VDM** and **VDM-OD** refer to the proposed *VDM-Mamba* and *VDM-OD-Mamba* variants.

Method	Vehicle				Pedestrian				Cyclist				mAP
	overall	0-30m	30-50m	50m+	overall	0-30m	30-50m	50m+	overall	0-30m	30-50m	50m+	
PointRCNN	52.1	74.5	40.9	16.8	4.3	6.2	2.4	0.9	29.8	46.0	20.9	5.5	28.7
PointPillars	68.6	80.9	62.1	47.0	17.6	19.7	15.2	10.2	46.8	58.3	40.3	25.9	44.3
SECOND	71.2	84.0	63.0	47.3	26.4	29.3	24.1	18.1	58.0	70.0	52.4	34.6	51.9
PV-RCNN	77.8	89.4	72.6	58.6	23.5	25.6	22.8	17.3	59.4	71.7	52.6	36.2	53.6
CenterPoint	66.8	80.1	59.6	43.4	49.9	56.2	42.6	26.3	63.5	74.3	57.9	41.5	60.1
PointPainting	66.2	80.3	59.8	42.3	44.8	52.6	36.6	22.5	62.3	73.6	57.2	40.4	57.8
LION	78.2	89.1	72.6	57.5	53.2	62.4	44.0	24.5	68.5	79.2	63.2	47.1	66.6
VDM-mamba	78.6	89.1	74.3	59.3	54.2	63.3	43.2	26.1	69.9	79.4	64.9	49.8	67.6

Table 5: Comparison with previous methods on ONCE validation set.

improving detection performance.

Results on Argoverse V2. As shown in Table 4, our proposed models, VDM-Mamba and VDM-OD-Mamba, achieve state-of-the-art detection performance on the Argoverse 2 validation set, reaching 42.3 mAP and 42.6 mAP, respectively. Compared with the strong baseline LION (Liu et al. 2024), VDM-Mamba yields a notable improvement of 0.8 mAP. Notably, VDM-OD-Mamba, which retains only the diffusion structure within the VDM module, still surpasses all previous approaches, highlighting the effectiveness of the diffusion mechanism. These results further demonstrate the strong representational capacity and scalability of the VDM module in large-scale point cloud scenarios.

Results on ONCE. VDM-Mamba also demonstrates superior performance on the ONCE dataset. It achieves detection accuracies of 78.6 mAP, 54.2 mAP, and 69.9 mAP on the *Vehicle*, *Pedestrian*, and *Cyclist* categories, respectively. The overall detection accuracy across all categories reaches 67.6 mAP, representing a +1.0 mAP improvement over the Mamba-based LION detector. These results establish VDM-Mamba as the new state-of-the-art (SOTA) on the ONCE benchmark.

Ablation Study

Ablation Study on Voxel Diffusion. To assess the contribution of voxel diffusion to detection performance, we con-

Diffusion	Waymo(3D AP/APH)L2		
	Vehicle	Pedestrian	Cyclist
No(LION)	68.8/68.3	77.3/72.6	74.7/73.8
Yes(VDM-OD)	70.3/69.9	78.2/73.8	76.0/75.0

Table 6: Detection results of the voxel diffusion module on the Waymo validation set (20% data). ”No” indicates that the original voxels are not diffused, and the detection results are entirely determined by LION(Liu et al. 2024) ”Yes” indicates that we only adopt the diffusion module from VDM, i.e., using sparse 3D spconv with a kernel size of 3 and a stride of 1.

duct ablation experiments on the Waymo validation set using a fixed voxel size of [0.32, 0.32, 0.1875]. We evaluate the model both with and without voxel diffusion. As shown in Table 6, introducing voxel diffusion improves the VDM-OD model by 1.3 mAPH (L2), underscoring its critical role in sequential detection frameworks. Moreover, on the nuScenes (Table 3) and Argoverse 2 (Table 4) datasets, we observe that under the *Only-diffusion* setting, the model still achieves higher detection accuracy, further validating the significant impact of voxel diffusion.

Ablation on Fine-grained Feature Aggregation. To further evaluate the fine-grained feature aggregation capability of VDM under more detailed voxel partitioning, we con-

Fine-grained	ONCE (Overall)				Waymo (Cyclist)			
	Vehicle	Pedestrian	Cyclist	mAP	AP (L1)	APH (L1)	AP (L2)	APH (L2)
Base (VDM-OD)	78.5	51.0	68.7	66.1	78.5	77.6	75.7	74.7
Fine (VDM)	78.6	54.2	69.9	67.6	79.1	78.1	76.2	75.2

Table 7: Ablation study on the ONCE and Waymo (20% data) dataset for fine-grained feature aggregation. *Base* denotes the detection results obtained by combining the VDM and Mamba network without fine voxel partitioning. *Fine* represents the results after applying fine-grained voxel partitioning.

ducted experiments by refining the voxel resolution. Specifically, we reduced the voxel size along the x and y axes to one-fourth of the original size, while keeping the resolution along the z -axis unchanged, with voxel diffusion still enabled.

As shown in Table 2, under this fine-grained aggregation setting, the model achieves a 0.5 APH (L2) improvement in detecting the *Pedestrian* category, indicating enhanced localization and recognition of small-scale objects. Furthermore, as reported in Table 7, on the ONCE dataset, the VDM-OD model exhibits inferior performance across all three categories when only voxel diffusion is applied. With the integration of fine-grained feature aggregation, the model achieves a 1.5 mAP gain, demonstrating the effectiveness of finer voxel partitioning in enhancing detection performance. When trained with 20% of the Waymo validation set, the VDM model also achieves higher detection accuracy for the *Cyclist* category.

Conclusion

We propose the Voxel Diffusion Module (VDM), which consists of a sparse 3D convolutional network, sparse residual blocks, and submanifold sparse convolution (SubM3D). This module diffuses voxelized point clouds via sparse 3D convolutions to increase the density of foreground voxels for more accurate object localization, while simultaneously performing spatial pre-aggregation of voxel features to provide spatial context for the subsequent serialized voxel sequences. To validate the effectiveness of our approach, we evaluate two model variants: VDM-LION (based on Mamba) and VDM-DSVT (based on Transformer). Experimental results demonstrate that VDM consistently improves performance in both SSMs-based and Transformer-based architectures. Notably, VDM-LION (SSMs) achieves state-of-the-art results on the Waymo, Argoverse 2, and ONCE datasets.

References

Bansal, M.; Krizhevsky, A.; and Ogale, A. 2018. Chauffeurnet: Learning to drive by imitating the best and synthesizing the worst. *arXiv preprint arXiv:1812.03079*.

Caesar, H.; Bankiti, V.; Lang, A. H.; Vora, S.; Liong, V. E.; Xu, Q.; Krishnan, A.; Pan, Y.; Baldan, G.; and Beijbom, O. 2020. nuscenes: A multimodal dataset for autonomous driving. In *Proceedings of the IEEE/CVF conference on computer vision and pattern recognition*, 11621–11631.

Chang, M.-F.; Lambert, J.; Sangkloy, P.; Singh, J.; Bak, S.; Hartnett, A.; Wang, D.; Carr, P.; Lucey, S.; Ramanan, D.; et al. 2019. Argoverse: 3d tracking and forecasting with rich maps. In *Proceedings of the IEEE/CVF conference on computer vision and pattern recognition*, 8748–8757.

Gu, A.; and Dao, T. 2023. Mamba: Linear-time sequence modeling with selective state spaces. *arXiv preprint arXiv:2312.00752*.

Jin, X.; Su, H.; Liu, K.; Ma, C.; Wu, W.; Hui, F.; and Yan, J. 2025. UniMamba: Unified Spatial-Channel Representation Learning with Group-Efficient Mamba for LiDAR-based 3D Object Detection. In *Proceedings of the Computer Vision and Pattern Recognition Conference*, 1407–1417.

Lang, A. H.; Vora, S.; Caesar, H.; Zhou, L.; Yang, J.; and Beijbom, O. 2019. Pointpillars: Fast encoders for object detection from point clouds. In *Proceedings of the IEEE/CVF conference on computer vision and pattern recognition*, 12697–12705.

Liu, Z.; Hou, J.; Wang, X.; Ye, X.; Wang, J.; Zhao, H.; and Bai, X. 2024. Lion: Linear group rnns for 3d object detection in point clouds. *Advances in Neural Information Processing Systems*, 37: 13601–13626.

Liu, Z.; Yang, X.; Tang, H.; Yang, S.; and Han, S. 2023. Flatformer: Flattened window attention for efficient point cloud transformer. In *Proceedings of the IEEE/CVF conference on computer vision and pattern recognition*, 1200–1211.

Mao, J.; Niu, M.; Jiang, C.; Liang, H.; Chen, J.; Liang, X.; Li, Y.; Ye, C.; Zhang, W.; Li, Z.; et al. 2021. One million scenes for autonomous driving: Once dataset. *arXiv preprint arXiv:2106.11037*.

Sun, P.; Kretzschmar, H.; Dotiwalla, X.; Chouard, A.; Patnaik, V.; Tsui, P.; Guo, J.; Zhou, Y.; Chai, Y.; Caine, B.; et al. 2020. Scalability in perception for autonomous driving: Waymo open dataset. In *Proceedings of the IEEE/CVF conference on computer vision and pattern recognition*, 2446–2454.

Vaswani, A.; Shazeer, N.; Parmar, N.; Uszkoreit, J.; Jones, L.; Gomez, A. N.; Kaiser, Ł.; and Polosukhin, I. 2017. Attention is all you need. *Advances in neural information processing systems*, 30.

Wang, H.; Shi, C.; Shi, S.; Lei, M.; Wang, S.; He, D.; Schiele, B.; and Wang, L. 2023. Dsvt: Dynamic sparse voxel transformer with rotated sets. In *Proceedings of the IEEE/CVF Conference on Computer Vision and Pattern Recognition*, 13520–13529.

Yang, H.; Wang, W.; Chen, M.; Lin, B.; He, T.; Chen, H.; He, X.; and Ouyang, W. 2023. Pvt-ssd: Single-stage 3d object detector with point-voxel transformer. In *Proceedings of*

the IEEE/CVF Conference on Computer Vision and Pattern Recognition, 13476–13487.

Yang, Z.; Sun, Y.; Liu, S.; and Jia, J. 2020. 3dssd: Point-based 3d single stage object detector. In *Proceedings of the IEEE/CVF conference on computer vision and pattern recognition*, 11040–11048.

Yin, T.; Zhou, X.; and Krahenbuhl, P. 2021. Center-Based 3D Object Detection and Tracking. In *Proceedings of the IEEE/CVF Conference on Computer Vision and Pattern Recognition (CVPR)*, 11784–11793.

Zhang, G.; Chen, J.; Gao, G.; Li, J.; Liu, S.; and Hu, X. 2024a. SAFDNet: A Simple and Effective Network for Fully Sparse 3D Object Detection. In *Proceedings of the IEEE/CVF Conference on Computer Vision and Pattern Recognition (CVPR)*, 14477–14486.

Zhang, G.; Fan, L.; He, C.; Lei, Z.; ZHANG, Z.-X.; and Zhang, L. 2024b. Voxel mamba: Group-free state space models for point cloud based 3d object detection. *Advances in Neural Information Processing Systems*, 37: 81489–81509.

Zhang, Y.; Hu, Q.; Xu, G.; Ma, Y.; Wan, J.; and Guo, Y. 2022. Not all points are equal: Learning highly efficient point-based detectors for 3d lidar point clouds. In *Proceedings of the IEEE/CVF conference on computer vision and pattern recognition*, 18953–18962.

Zhou, Y.; and Tuzel, O. 2018. Voxelnet: End-to-end learning for point cloud based 3d object detection. In *Proceedings of the IEEE conference on computer vision and pattern recognition*, 4490–4499.

Zhu, Y.; Mottaghi, R.; Kolve, E.; Lim, J. J.; Gupta, A.; Fei-Fei, L.; and Farhadi, A. 2017. Target-driven visual navigation in indoor scenes using deep reinforcement learning. In *2017 IEEE international conference on robotics and automation (ICRA)*, 3357–3364. IEEE.